Advanced FO Membranes from Newly Synthesized CAP Polymer for Wastewater Reclamation through an Integrated FO-MD Hybrid System

Jincai Su, Rui Chin Ong, Peng Wang, and Tai-Shung Chung
Dept. of Chemical and Biomolecular Engineering, National University of Singapore, 4 Engineering Drive 4, Singapore 117576

Bradley J. Helmer, and Jos S. de Wit
Eastman Chemical Company, P.O. Box 1972, Kingsport, TN 37662

DOI 10.1002/aic.13898
Published online August 20, 2012 in Wiley Online Library (wileyonlinelibrary.com).

A new cellulose acetate propionate (CAP) polymer has been synthesized and used to prepare high-performance forward osmosis (FO) membranes. With an almost equal degree of substitution of acetyl and propionyl groups, the CAP-based dense membranes show more balanced physicochemical properties than conventional cellulose acetate (CA)-based membranes for FO applications. The former have a lower equilibrium water content (6.6 wt. %), a lower salt diffusivity (1.6×10^{14} m^2 s^{-1}) and a much lower salt partition coefficient (0.013) compared with the latter. The as-prepared and annealed CAP-based hollow fibers have a rough surface with an average pore radius of 0.31 nm and a molecular weight cut off of 226 Da. At a transmembrane pressure of 1 bar, the dual-layer CAP-CA hollow fibers show a pure water permeability of 0.80 L m^{-2} h^{-1} bar^{-1} (LMH/bar) and a rejection of 75.5% to NaCl. The CAP-CA hollow fibers were first tested for their FO performance using 2.0 M NaCl draw solution and deionized water feed. An impressive water flux of 17.5 L m^{-2} h^{-1} (LMH) and a reverse salt flux of 2.5 g m^{-2} h^{-1} (gMH) were achieved with the draw solution running against the active CAP layer in the FO tests. The very low reverse salt flux is mainly resulting from the low salt diffusivity and salt partition coefficient of the CAP material. In a hybrid system combining FO and membrane distillation for wastewater reclamation, the newly developed hollow fibers show very encouraging results, that is, water production rate being 13–13.7 LMH, with a $MgCl_2$ draw solution of only 0.5 M and an operating temperature of 343 K due to the incorporation of bulky propionyl groups with balanced physiochemical properties. *AIChE J,* 59: 1245–1254, 2013
Keywords: cellulose acetate propionate (CAP), forward osmosis, dual-layer hollow fiber, wastewater reclamation, FO-MD hybrid system

Introduction

Forward osmosis (FO) is an emerging technology that shows great potential for water treatment,[1–5] power generation,[6,7] protein concentration,[8] and agricultural fertigation.[9] However, breakthroughs on FO membranes and draw solutes are urgently needed in order to fully commercialize the FO technology for broader aspects. Current FO research mainly focuses on four areas, that is, (1) molecular design of new membrane materials with superior FO performance,[10–16] (2) synthesis of low cost and recyclable novel draw solutes that offer high osmotic pressures,[17,18] (3) investigation of FO membrane fouling and efficient cleaning methods,[19,20] and (4) exploration of hybrid systems and development of new applications.[2,9]

A suitable membrane is the 1st key component of the FO process. Several FO membranes have been reported including: (1) flat sheet membranes;[10–12,21–23] (2) single- and dual-layer hollow fibers;[13,24,25] (3) thin film composite (TFC) polyamide membranes;[14,26] (4) layer-by-layer assembly;[15] and (5) biomimetic membranes.[16] Comparing TFC polyamide membranes with phase inversion membranes, the former generally has a greater water flux than the latter. However, the thin TFC polyamide layer might detach from its porous substrate if the draw solution runs against the membrane active layer (i.e., pressure retarded osmosis [PRO] mode) because there would be a net flow of water from the feed to the draw solution. This water flow can damage the membrane and deteriorate the performance, and is a serious problem for long term operation in real applications. Moreover, backwashing of the fouled TFC FO membrane may have a similar effect. Running the draw solution against the substrate (FO mode) would not create such a problem, but this membrane orientation may significantly reduce the driving force due to severe internal concentration polarization (ICP).[27] On the contrary, FO membranes prepared from conventional phase inversion method would not have such a risk and would be more stable in real cases. Comparatively,

Correspondence concerning this article should be addressed to T.-S. Chung at chencts@nus.edu.sg.

Table 1. Properties of the CAP Polymer and Dense CAP Membranes

Sample	DS (OH)	DS (Pr)	DS (Ac)	Mw (kDa)	D_sK_s 10^{+16} (m^2 s^{-1})	K_s	D_s 10^{+13} (m^2 s^{-1})	C_w (wt. %)
CAP	0.59	1.23	1.18	105.8	2.05	0.013	0.16	6.6

DS: degree of substitution
OH: hydroxyl
Pr: propionyl
Ac: acetyl

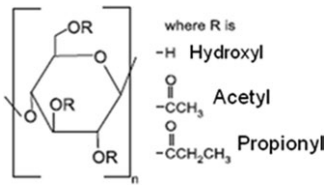

hollow fiber configuration would be more realistic for FO applications considering the fact that FO processes are normally running at atmospheric pressure. Furthermore, hollow fiber configuration offers a higher packing density (i.e., high surface area per unit material mass) and has the advantage of self-support as well as less demands for pretreatment and maintenance.[28,29]

The recycle of draw solutes is another essential element for the success of the FO technology. The osmotic pressure gradient across the FO membrane between the draw solution and the feed solution acts as the driving force for the FO process. The draw solution must be recycled because it is diluted after drawing solvent (normally water) from the feed. Several approaches have been proposed to reconcentrate the draw solution such as nanofiltration (NF),[30] reverse osmosis (RO),[2,3] FO,[31] or membrane distillation (MD).[32] Although NF and RO are applicable, using high hydraulic pressures would raise a lot of concerns such as high capital and operation costs as well as fouling.

Thermal process is an alternative. In the study of McCutcheon et al.,[1] an ammonium bicarbonate solution was used as the draw solution in the FO desalination process. After the FO process, the diluted ammonium bicarbonate solution was heated to 333 K and it would decompose into ammonia and carbon dioxide gases. Product water was obtained after separating the two gases from water. However, another research group observed the difficulties to completely redissolve the carbon dioxide and reproduce the draw solution.[33] A hybrid FO-MD system may be more cost effective if waste or low quality heat is available nearby water reuse or desalination plants. Wang et el.[32] have employed a hybrid FO-MD system to regenerate draw solutes for the concentration of protein solutions, while Yen et al.[34] has used a similar system to recycle their newly developed draw solutes.

The main objective of this work is to design novel high-performance dual-layer hollow fiber FO membranes made from a proprietary cellulose acetate propionate (CAP) polymer for wastewater reclamation through a FO-MD hybrid system. The proprietary CAP out-performs the conventional cellulose acetate (CA) and cellulose triacetate (CTA) polymers in terms of water flux and salt rejection in FO processes. The motivations for synthesizing this new CAP are as follows. As observed in the literature, CA-based FO membranes show acceptable water fluxes but unsatisfactory rejection of NaCl draw solutes, while CTA-based FO membranes usually show high NaCl rejection but suffer from low water fluxes. Aiming at achieving balanced water flux and salt rejection properties, this CAP was synthesized with relatively bulkier and more hydrophobic propionyl groups. Specifically, the newly synthesized CAP polymer differs from currently available CA and CAP polymers in a way that it contains an almost equal degree of substitution of acetyl and propionyl groups and a lower hydroxyl level. The dual-layer coextrusion technology was chosen because it offers the flexibility to create a very thin and dense CAP film attached to a highly porous and hydrophilic CA sublayer. This type of dual-chemistry morphology cannot be accomplished by using the conventional single-layer spinning technology. Such a membrane fabrication method is favorable for improving the FO performance because the active dense layer can increase the salt rejection, while the porous inner layer can reduce the ICP within the sublayer in the FO mode.[35] To the best of our knowledge, this is the first trial to use a FO-MD hybrid system for wastewater reclamation.

Experimental

Materials

CA-398-30 and proprietary CAP polymers for FO membranes were supplied by our collaborator, Eastman Chemical Company and the properties of CAP are shown in Table 1. Polyvinylidene fluoride (PVDF) HSV900 for MD membranes was provided by Arkema Corp. Analytical reagent grade acetone, formamide, *N*-methyl-2-pyrrolidone (NMP), dimethylformamide (DMF), isopropanol, NaCl, $MgCl_2{\cdot}6H_2O$, $ZnCl_2$ and $MgSO_4$ were purchased from Merck (Germany) while ethylene glycol (EG), diethylene glycol (DEG), triethylene glycol (TEG), glycerol, glucose, and polytetrafluoroethylene (PTFE) particles (<1 μm) were supplied by Sigma Aldrich. CAP, CA, PVDF, and PTFE were dried overnight under vacuum prior to use. $CoCl_2{\cdot}6H_2O$ was purchased from Acros Organics and $FeCl_2{\cdot}4H_2O$ were supplied by Fluka. Deionized (DI) water (PURELAB, Elga) was used to prepare the solutions.

Viscosity profile and phase diagram

A series of CAP solutions in NMP were prepared and the viscosity of each solution was measured using a Cone-and-Plate ARES Rheometric Scientific Rheometer at a shear rate of 10 s^{-1}. For viscosity measurements, NMP instead of acetone was used as the solvent in order to avoid the influence from solvent evaporation. Another five CAP solutions were prepared in small glass bottles using acetone/formamide mixture as the solvent. Water was used as a nonsolvent and the phase inversion of the CAP/acetone/formamide solutions was studied. The phase diagram was constructed based on the solution concentration and the amount of water added for the phase inversion.

Table 2. Spinning and Annealing Conditions of the CAP-CA Dual-Layer Hollow Fibers

Outer dope solution (wt. %)	CAP/Acetone/Formamide (27/43.8/29.2)
Outer dope flow rate (L h^{-1})	0.03
Inner dope solution (wt. %)	CA(398)/Acetone/Formamide (18/49.2/32.8)
Inner dope flow rate (L h^{-1})	0.18
Bore fluid, temperature (K)	NMP/Water (90/10 wt.%), 298 K
Bore fluid flow rate (L h^{-1})	0.24
Length of air gap (m)	0.05
External coagulant, temperature (K)	Water, 298 K
Spinning humidity (%)	60∼ 70%
Take up speed (m s^{-1})	0.23
Annealing	Fibers immersed in a water bath at 358 K for 0.083 h

Formation of CAP dense membranes

To examine the equilibrium water content, salt diffusivity and salt partition coefficient, CAP dense membranes with thicknesses of 1.5×10^{-5} and 1.5×10^{-4} m were fabricated. The thinner dense membrane (1.5×10^{-5} m) was cast from a dope solution of CAP (12 wt. %) dissolved in DMF. After casting using a 100 μm casting knife on a smooth glass substrate, the nascent film was subjected to solvent evaporation at 353 K for 24 h in an oven. The membrane was then peeled off and further dried under vacuum in a vacuum oven with gradually increasing the temperature from 353 to 423 K at a heating rate of 25 K every 2 h. Subsequently, the membrane was kept overnight in a vacuum oven at 423 K to completely remove the residual solvent. The thicker dense membrane (1.5×10^{-4} m) was prepared via ring casting. Certain amount of CAP (4 wt. %) dissolved in acetone was poured evenly into a Petri dish and the solvent evaporated at room-temperature for 48 h before the membrane was peeled off. Both types of dense membranes were thermally annealed at 468 K (i.e., about 20 K above Tg) for 0.33 h under vacuum and then immediately quenched to room-temperature.

Formation of CAP-CA dual-layer hollow fiber membranes

A mixture of acetone and formamide was used as the solvent to prepare CAP and CA dope solutions for spinning. To avoid the evaporation of acetone, the mixing and dissolving were conducted in blue-cap bottles sealed with parafilm. The blue-cap bottles were then mounted on a rotator (STR4, Stuart) and were rotated for several days until homogeneous solutions were obtained. The compositions of the CAP and CA dope solutions are given in Table 2.

CAP-CA dual-layer hollow fibers were fabricated through a dry-jet wet-spinning process[19] and the corresponding spinning conditions are given in Table 2. Briefly, the CAP solution, the CA solution and the bore fluid (internal coagulant) were separately delivered to the spinneret through high-precision pumps (ISCO-100DX, ISCO Inc.) and simultaneously extruded through the spinneret as shown in Figure 1. The nascent fibers were immersed in tap water for several days to remove the residual solvents before thermal annealing in a water bath at 358 K for 0.083. The annealed hollow fibers were immersed in a mixture of glycerol/water (50/50 wt. %) for 48 h in order to avoid the collapse of surface pores and thoroughly air-dried at room-temperature. For module fabrication, 20 pieces of hollow fibers with a length of around 0.3 m each were bundled into a Φ3/8 in. perfluoroalkoxy tubing and the two ends were sealed with epoxy resin. The CAP-CA hollow fiber membrane module had a filtration area of about 8×10^{-3} m^2.

Formation of PVDF single-layer hollow fiber membranes

PVDF single-layer hollow fiber membranes for MD were developed as follows. The dope solution was prepared by dissolving PVDF and PTFE particles in a mixture of NMP/EG. The composition of the dope, detailed spinning conditions and post-treatment are listed in Table 3. After spinning, the as-spun PVDF fibers were immersed in tap water for several days to remove the residual solvent and then dried overnight in a freeze-dryer (S61-Moudulyo-D, Thermo Electron Cor.) at 223 K. A MD membrane module with 15 fibers was fabricated with an effective area of 8×10^{-3} m^2.

Characterizations

Properties such as the equilibrium water content, salt partition coefficient and density were determined from the thicker dense membranes (1.5×10^{-4} m). The density was measured using the density kit according to the Archimedean principle and calculated using the follow equation:

$$\rho = \frac{W_{\text{air}}}{W_{\text{air}} - W_{\text{liqid}}} \times \rho_0 \tag{1}$$

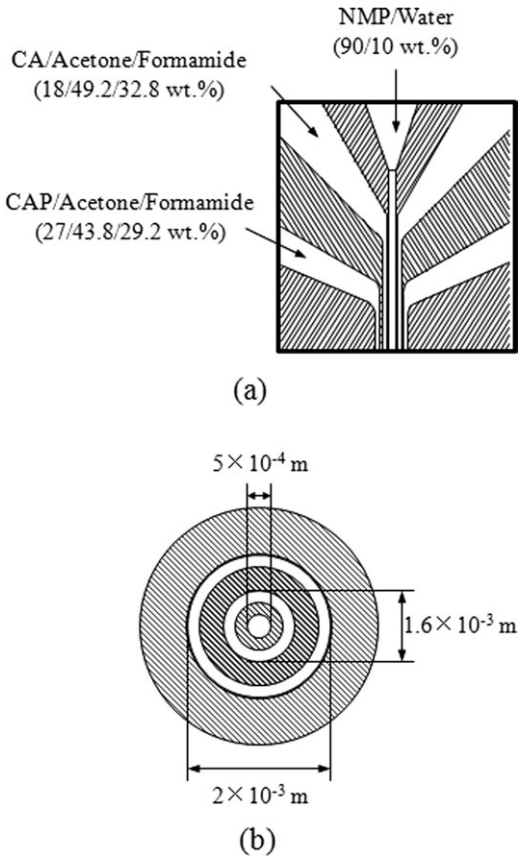

Figure 1. Schematic diagram of the dual-layer spinneret and flow channels of the dope solutions and bore fluid for the hollow fiber spinning.

(a) front view; (b) top view.

Table 3. Spinning and Post Treatment Conditions and Dimensions of the PVDF-PTFE Single-Layer Hollow Fibers

Dope solution (wt. %)	PVDF (HSV900)/PTFE/NMP/EG (14.5/3.3/67.7/14.5)
Dope flow rate (L h^{-1})	0.21
Bore composition (wt. %)	NMP/water (70/30)
Bore fluid flow rate (L h^{-1})	0.12
External coagulant (wt. %)	IPA/water (60/40)
Length of air gap (m)	0.02
Spinning humidity (%)	60∼70
Take up speed (m s^{-1})	Free fall
Post treatment	Solvent exchange (water) & freeze dry
OD/ID (m)	$9.03\times10^{-4}/6.16\times10^{-4}$

where ρ and ρ_0 are the densities of the dense membrane and the auxiliary liquid (ethanol) while W_{air} and W_{liquid} are the weights of the dense membrane in air and the auxiliary liquid, respectively. To measure the equilibrium water content, dry membrane samples were weighted and immersed in ultra-pure water for 72 h for water uptake. Before weighing the wet membrane samples, water on the membrane surface was gently wiped off using tissue paper. The equilibrium water content, C_w, was calculated using the following equation:

$$C_w = \frac{W_{wet} - W_{dry}}{W_{dry}} \times 100\% \quad (2)$$

where the W_{dry} and W_{wet} are the weight of the dry and wet membranes, respectively. At least three membrane samples were measured and the average equilibrium water content was taken.

The salt partition coefficient, K_s, was determined by measuring the salt uptake by the thicker dense membranes (1.5×10^{-4} m). Membrane samples with known weights were firstly immersed in ultra-pure water for 72 h to wash away any residual salt in them. Then, the samples were wiped dry using tissue paper and immersed into a 3.5 wt. % NaCl solution for salt uptake. The membrane samples were taken out from the NaCl solution after 72 h and their surfaces were gently rinsed with ultrapure water for three times. Subsequently, the membrane samples were cut into small pieces and immersed into 3×10^{-3} L ultrapure water to desorb the absorbed salt by continuously stirring for 72 h. The chloride ion content in the solution was measured using an ion chromatography (Metrohm Model 702). The salt partition coefficient, K_s, was calculated using the equation shown below:

$$K_s = \frac{C_{membrane}}{C_{solution}} \quad (3)$$

where $C_{membrane}$ and $C_{solution}$ are the concentrations of NaCl in the dense membrane and the solution, respectively.

The salt diffusion coefficient, D_s, was measured from the thinner dense membranes (1.5×10^{-5} m) using a static FO permeation cell as shown in Figure 2. The membrane sample was clamped in between two solution chambers which were initially filled with 0.035 L ultra-pure water and 0.035 L 3.5 wt. % NaCl solution, respectively. Due to the concentration difference between the two chambers, certain amount of NaCl would diffuse through the membrane and increase the NaCl concentration in the water chamber. Since there is the osmotic pressure difference across the membrane, certain amount of water would permeate through the membrane and decrease the water volume in the same chamber. After stabilizing for 0.5 h, a sample of 1.5×10^{-3} L was taken from the water chamber and its NaCl concentration was measured using the ion chromatography. The system was then allowed for NaCl diffusion for 72 h with the two chambers continuously stirred in order to minimize the influence of concentration polarization. At the end of the experiment, the amount of ultra pure water left in the water chamber was measured using a measuring cylinder and its concentration was determined using the ion chromatography. The final concentration of the NaCl solution in another chamber was also measured using a calibrated conductivity meter (Lab 960, Schott). The salt diffusion coefficient, D_s, was calculated using the following equation:[36]

$$J_s = -D_s K_s \frac{C_{s,w} - C_{s,s}}{\Delta x} \quad (4)$$

where J_s is the salt flux, $C_{s,w}$ is the final salt concentration in the water chamber, $C_{s,s}$ is the final salt concentration of the NaCl solution, and Δx is the thickness of the dense CAP membrane.

For morphological studies, several pieces of annealed CAP-CA hollow fibers were freeze-dried and fractured cryogenically in liquid nitrogen and coated with platinum using a JOEL JFC-1300 sputtering device. The cross section and membrane surface were inspected using Field Emission Scanning Electron Microscopy (FESEM, JOEL JSM-6700).

CAP-CA hollow fiber membranes were firstly subjected to the measurement of pure water permeability (PWP) and then subjected to 0.02% neutral solutes (ethylene glycol, diethylene glycol, triethylene glycol, and glucose) and NaCl separation tests under a transmembrane pressure of 1 bar. In these tests, DI water or the feed solution was circulated against the membrane active layer. The concentrations of the neutral solutes in the feed and the permeate were determined using a total organic carbon analyzer (TOC-V_{CSH}, Shimadzu). The concentrations of NaCl in the feed and the permeate were measured using the conductivity meter. The effective solute rejection coefficient R_E (%):

$$R_E = \left(1 - \frac{C_P}{C_f}\right) \times 100\% \quad (5)$$

The mean pore radius and the pore radius distribution were obtained from the rejections to the neutral solutes. A detailed description of the pore structural characterization was given elsewhere.[25]

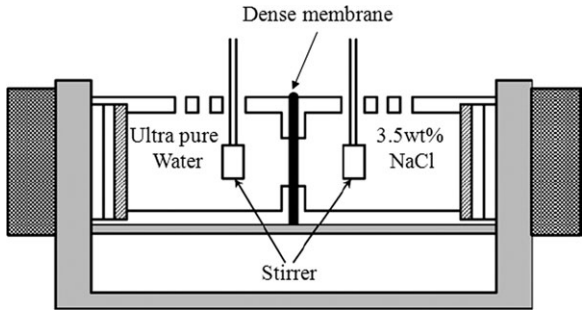

Figure 2. Static FO permeation cell for salt diffusivity measurements.

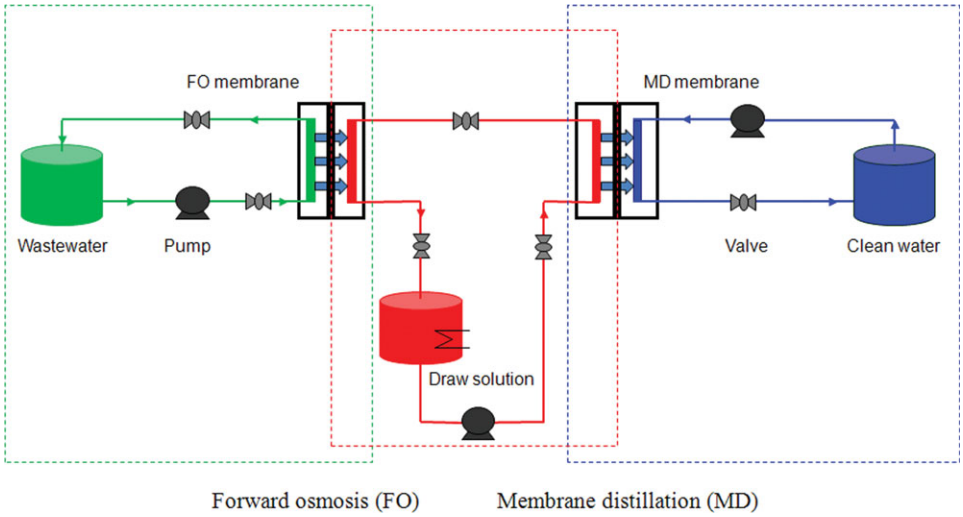

Figure 3. Schematic diagram of the lab-scale FO-MD hybrid system.

[Color figure can be viewed in the online issue, which is available at wileyonlinelibrary.com].

FO tests

The performance of CAP-CA dual-layer hollow fiber membranes was tested using a lab-scale FO setup described elsewhere.[25] FO tests were firstly conducted using 0.5–2.0 M NaCl draw solutions and DI water feed to determine the water flux and the reverse salt flux. As salts are the draw solutes in this study, the term "reverse salt flux" instead of reverse solute flux is used. The flow rates were 30 and 12 L h^{-1} at the shell and lumen sides, respectively. The water permeation flux, J_w, was determined based on the weight change of the feed and the effective membrane area as follows:

$$J_w = \frac{\Delta m}{\Delta t}\frac{1}{A_m} \tag{6}$$

where A_m is the effective membrane area and Δm is the weight of water permeated from the feed to the draw solution over a predetermined time Δt during FO tests. The value of J_s was determined from the increase in the feed conductivity:

$$J_s = \frac{[(C_t V_t - (C_0 V_0)]M_w}{\Delta t}\frac{1}{A_m} \tag{7}$$

where C_0 and V_0 are the initial salt concentration and the initial volume of the feed, respectively, while C_t and V_t are the salt concentration and the volume of the feed over a predetermined time Δt, respectively, during FO tests.

The FO-MD hybrid system for wastewater reclamation

A lab-scale FO-MD hybrid system as shown in Figure 3 was used for wastewater reclamation and the synthetic wastewater contained an equal weight amount of heavy metal ions, that is, $FeCl_2$, $CoCl_2$, $MgSO_4$, and $ZnCl_2$. At the FO side, the feed solution (DI water or wastewater) was circulated through the lumen side of CAP-CA hollow fibers. At the MD side, the distilled water was circulated at the lumen side of PVDF hollow fibers. The temperatures of the permeate at the PVDF module and the feed solution at the FO side were set at 298 K. A 0.5 M $MgCl_2$ draw solution was circulated at the shell sides of the FO and the MD membrane modules, respectively, with flowing first through the MD module and then through the FO module before going back to the draw solution tank. It should be noted that $MgCl_2$ instead of NaCl was used as the draw solute in the hybrid system. The purpose was to avoid severe reverse salt fluxes because the draw solutes would have higher diffusivity at elevated temperatures. Another concern was that there would not be any risk of scaling using $MgCl_2$ draw solutes.[37] The inlet temperature of the draw solution at the MD module was 343 K. In both membrane modules, all the solutions flowed cocurrently and upward along corresponding channels. The weight changes of the feed solution in the FO process and the permeate (distillated water) in the MD process were monitored.

Results and Discussion

Equilibrium water content, salt diffusivity, and salt partition coefficient

Solubility and diffusivity to solutes and solvents are important inherent properties which determine the membrane selectivity.[36] For the CAP polymer with degrees of substitution DS (OH) = 0.59, DS(Pr) = 1.23 and DS(Ac) = 1.18, the equilibrium water content determined from dense membranes is 6.6 wt. % while the diffusivity for NaCl is 1.6×10^{-14} m^2 s^{-1} and the salt partition coefficient is 0.013. As reported by Soltanieh,[36] the equilibrium water content, the diffusivity for NaCl and the salt partition coefficient for conventional CA membranes are 12.0–13.6 wt %, $0.86–5.1 \times 10^{-13}$ m^2 s^{-1}, and 0.013–0.038, respectively. It is evident that the CAP membrane shows lower equilibrium water content. This is resulting from the addition of bulkier propionyl group with increased hydrophobicity[38] and decrease in hydroxyl content. However, the newly synthesized polymer has a lower diffusivity for NaCl and a lower partition coefficient because of the existence of propionyl group.

Viscosity profile and phase diagram

The viscosity increases with increasing CAP concentration and the increment is small when the CAP concentration is lower than 15 wt. % (Figure 4a). After 15 wt. % concentration, a exponential increase in viscosity can be observed because of rapid chain entanglement. Two extrapolation lines can be drawn as illustrated in Figure 4a and the cross point corresponds to the critical concentration.[39] Membranes prepared from solutions with a concentration higher than the

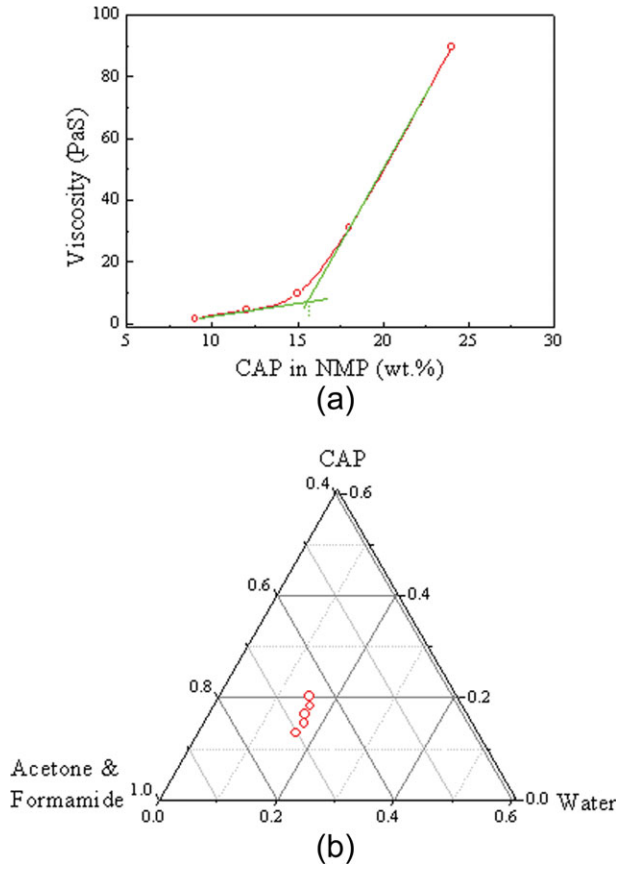

Figure 4. (a) Viscosity of CAP/NMP solutions and (b) the phase diagram of CAP/(Acetone and Formamide)/water system.

[Color figure can be viewed in the online issue, which is available at wileyonlinelibrary.com].

critical concentration may have fewer defects for separation following the solution-diffusion mechanism. A CAP concentration of 27 wt. % was used for dual-layer hollow fiber spinning in order to eliminate the risk to form defects.

Figure 4b gives the ternary phase diagram of the CAP/(acetone and formamide)/water system at 298 K. The cloud points are far away from the polymer-solvents axis, indicating that this system needs more water to induce CAP precipitation as compared with other polymer solutions such as PVDF/NMP and polysulfone/NMP.[40,41] This phenomenon is similar to that observed for the CA/NMP/water system.[21]

Morphology and topology of CAP membranes

As shown in Figure 5, the outer CAP layer is very thin and dense, while the inner CA layer is thick and porous. There is no delamination between them. A number of finger-like macrovoids are observed across the inner support layer. These macrovoids are favorable for enhancing the mass transfer by offerring a resistance-free support layer because they have "open-cell" skins. The outer layer consists of a dense selective skin and spongy like underneath, as illustrated by the FESEM picture at a high mangification. It should be noted that there are some cracks on the outer surface and these cracks are caused by electron beams. As observed during FESEM inspection, the CAP-CA hollow fiber samples are easily burnt when the magnification is over $\times$10,000 and a similar phenomenon has been reported for other cellulose esters.[42]

The atomic force microscope (AFM) images (Figure 6) show that a large number of very tiny nodules exist at the outer surface of the hollow fibers. This is an indication that the CAP layer offers a high surface area for water to permeate through. The mean roughness of the outer surface is 4.8×10^{-9} m and the maximum vertical distance between the highest and lowest data points is 8.3×10^{-8} m. The high surface roughness is beneficial to improve mass transfer.[43] Although it may encourage fouling, fouling in FO processes is not as serious as pressure-driven processes such as RO and the water flux of the fouled membranes can be almost 100% recovered with a simple cleaning method.[19]

Membrane characterization through NF

The PWP and NaCl rejection achieved by the CAP-CA hollow fibers are 0.80 LMH/bar and 75.5%, respectively (Table 4). From the rejections to neutral solutes (e.g., EG, DEG,

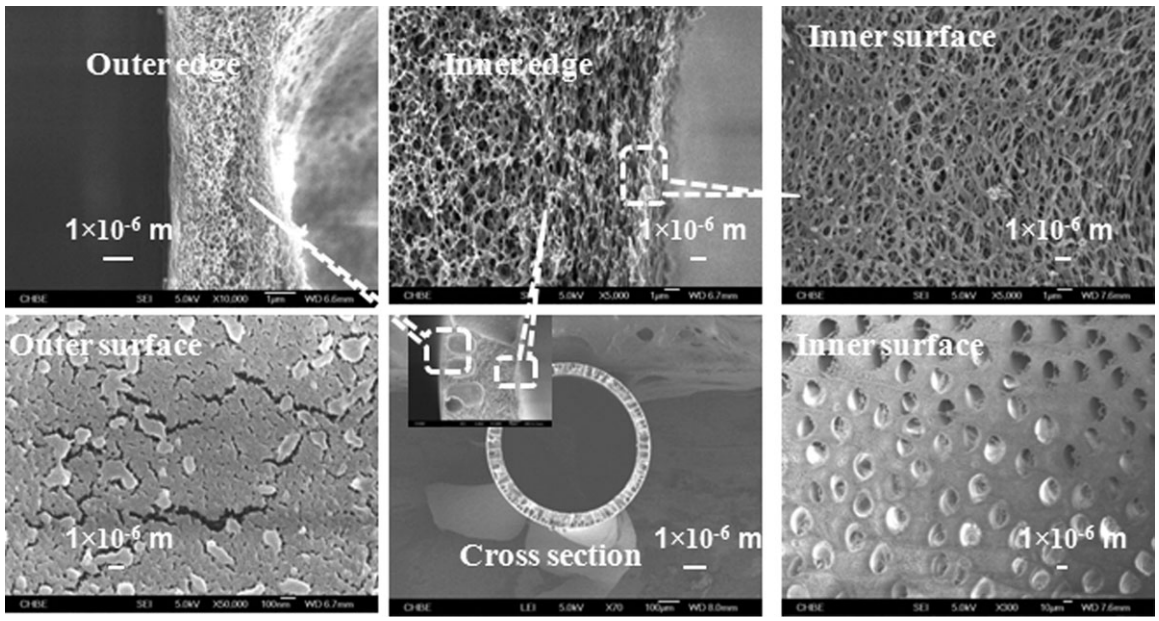

Figure 5. Morphology of the CAP-CA dual-layer hollow fibers.

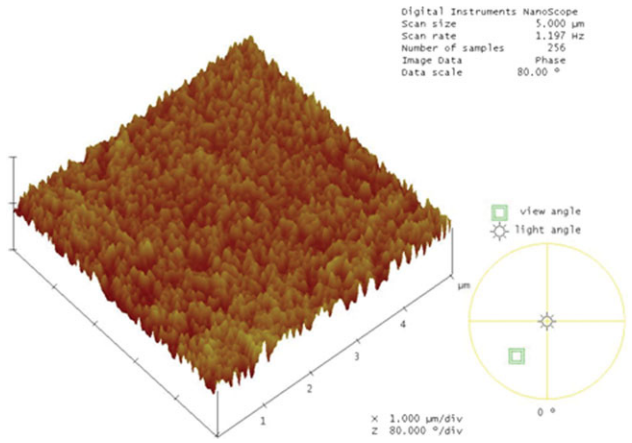

Figure 6. AFM image of the CAP-CA dual-layer hollow fibers.

[Color figure can be viewed in the online issue, which is available at wileyonlinelibrary.com].

TEG, and Glycerol) shown in Figure 7a, the mean pore radius and molecular weight cut off (MWCO) of the hollow fibers are determined as 0.31 nm and 226 Da, respectively. It can be seen from Figure 7b that the surface pores of the CAP-CA hollow fibers fall in a very narrow range of 0.18–0.5 nm. The quantity and radius of pores within the active layer are very important for FO membranes because they govern the permeation rates of water and the draw solutes.

Performance in the FO process

With 0.5–2.0 M NaCl draw solutions and DI water feed, the water fluxes achieved by the CAP-CA dual-layer hollow fibers are in the range of 5.3–17.6 LMH in the PRO mode with reverse salt fluxes of 0.7–2.5 gMH (Figure 8). In the FO mode, lower water fluxes of 3.5–8.9 LMH and reverse salt fluxes of 0.5–1.3 gMH are obtained. The reduced water fluxes in the FO mode are due to the great impact of ICP.[25,27] One very encouraging observation is that the CAP-CA hollow fibers show much better performance than the CA-based membranes.[21,25] For example, flat CA membranes from Zhang et al.[21] had a water flux of 11.1 LMH with a reverse salt flux of about 6.9 gMH based on 2.0 M NaCl draw solution and DI water feed in the PRO mode. Under similar testing conditions, single-layer CA hollow fibers from Su et al.[25] showed a similar reverse salt flux of 2.3 gMH but a much lower water flux of 5.6 LMH. It is believed because the propionyl group is bulkier and more hydrophobic than the acetyl group, the newly developed CAP has an enhanced water flux and salt retention.[38] Generally, high hydrophobicity is not expected for FO membranes since it is not favorable for increasing the water flux. Interestingly, high content of propionyl and acetyl groups and equal amount of them offer balanced physicochemical properties which not only guarantee a high salt retention but also maintain a high water permeation flux.

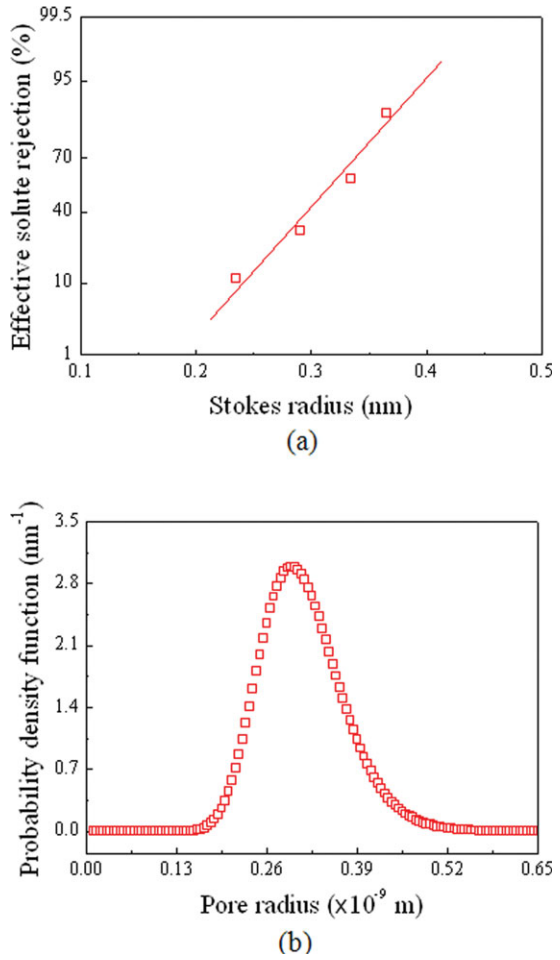

Figure 7. (a) Solute rejection and (b) probability density function curve for characterizing the pore structure of the CAP-CA dual-layer hollow fibers.

[Color figure can be viewed in the online issue, which is available at wileyonlinelibrary.com].

Wastewater reclamation through a FO-MD hybrid system

The FO-MD hybrid system is firstly run with 0.5 M $MgCl_2$ draw solution and DI water feed at 343 K. The water fluxes created by FO and MD membranes are 19.9 and 16.2 LMH, respectively, with corresponding reverse salt fluxes of 1.3 and 1.7 gMH in the FO process. The water fluxes for both processes can be higher with increasing the operating temperature. However, a higher operating temperature is not preferred in this study because the performance of CAP-CA hollow fibers may be significantly affected at temperatures higher than 343 K due to annealing effect.

Figure 9 shows the water flux in both FO and MD processes as a function of heavy metal ion concentration using synthetic wastewater solutions containing 0.05–1 $\times$ 10^{-3} Kg

Table 4. Dimensions, Mean Pore Radius, MWCO, PWP and NaCl Rejection of the CAP-CA Dual-Layer Hollow Fibers

Fiber OD (m)	Fiber ID (m)	Mean Pore Radius (nm)	MWCO (Da)	PWP @ 1 bar (LMH/bar)	Rejection to NaCl @ 1 bar (%)
8.4×10^{-4}	7.1×10^{-4}	0.31	226	0.80	75.5

MWCO: molecular weight cut-off
PWP: pure water permeability

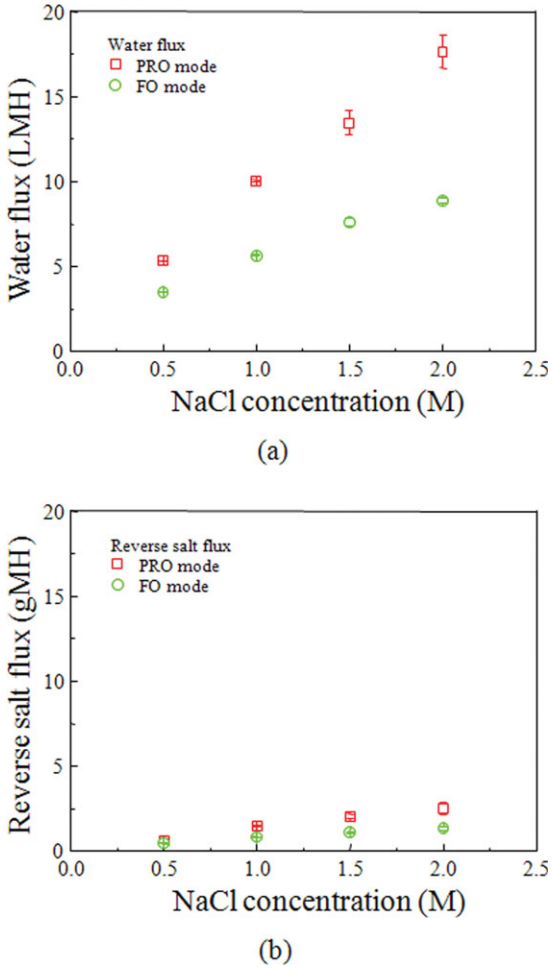

Figure 8. FO performance of the CAP-CA dual-layer hollow fibers: (a) water flux; (b) reverse salt flux.

[Color figure can be viewed in the online issue, which is available at wileyonlinelibrary.com].

L^{-1} heavy metal ions (i.e., equal weight amount of $FeCl_2$, $ZnCl_2$, $MgSO_4$, and $CoCl_2$) as the feed. The water flux decreases with increasing the feed solution concentration. In

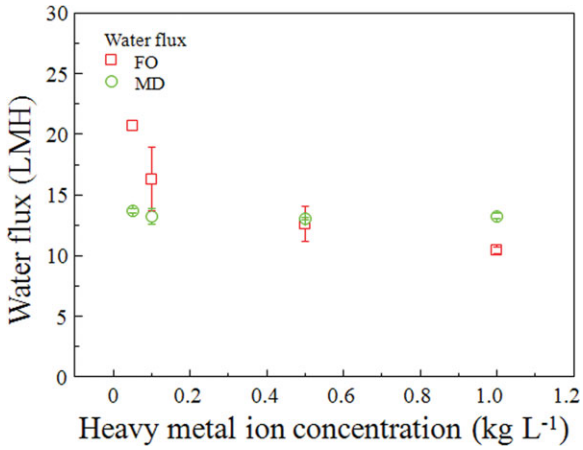

Figure 9. Water fluxes achieved in the FO-MD hybrid system for wastewater reclamation.

[Color figure can be viewed in the online issue, which is available at wileyonlinelibrary.com].

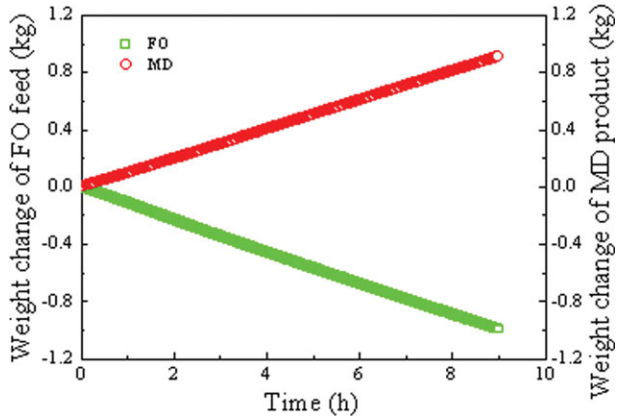

Figure 10. Weight changes observed from the FO and MD membranes in the FO-MD hybrid system for wastewater reclamation.

Draw solution: 0.5 M $MgCl_2$; Feed solutions: synthetic wastewater containing 500 mg L^{-1} $FeCl_2$, $CoCl_2$, $MgSO_4$, and $ZnCl_2$. [Color figure can be viewed in the online issue, which is available at wileyonlinelibrary.com].

the FO process, more severe ICP occurs at higher heavy metal ion concentrations which accounts for the reduction in water flux. Due to the thermally driven characteristics of the MD process, its water permeation rate is insensitive toward metal ion concentration. Hence, the water flux observed at the MD membrane stays nearly constant at different feed concentrations. When the feed solution contains 5×10^{-5} or 1×10^{-4} Kg L^{-1} heavy metal ions, the water production rate of the FO membrane is higher than that of the MD membrane. At a feed concentration of 5×10^{-4} Kg L^{-1}, the FO and MD membranes have similar water fluxes, that is, 12.6 LMH and 13.0 LMH, respectively. As one can see in Figure 10, the weight changes in both processes are almost the same. Equal or similar water flux for both processes is preferable, and the production rate of this hybrid system can be easily sustainable. These observations prove that the FO-MD hybrid system has a great potential for wastewater reclamation. The CAP-CA dual-layer hollow fiber membrane is also a good candidate for this system because it generates an attractive water production rate and a reasonably low draw solute leakage.

Conclusions

We have developed high-performance dual-layer hollow fiber FO membranes from a newly synthesized CAP polymer. The as-prepared and annealed membranes have a very dense selective layer and highly porous sublayer structure. With an equal degree of substitution of acetyl and propionyl groups, the CAP-based dense membranes show a lower equilibrium water content as well as a lower salt diffusivity and salt partition coefficient compared with CA-based membranes. The reduced equilibrium water content may influence the water flux, but the very low reverse salt flux that is related to the reduced salt diffusivity and salt partition coefficient would add significant values to the FO membranes and make this CAP polymer much more attractive than CA. The CAP-based hollow fibers have surface pores with an average radius of 0.31 nm and a MWCO of 226 Da. In the FO process, these hollow fibers create much higher water fluxes and lower reverse salt fluxes than CA-based membranes.

This observation verifies that high content of propionyl and acetyl groups and their equal degree of substitution are very important for CAP-based FO membranes. The very encouraging FO performance obtained through a FO-MD hybrid system discloses that the newly developed CAP-CA hollow fiber membranes have great potential for the application in wastewater reclamation.

Acknowledgments

The authors thank Eastman Chemical Company (USA) support with a grant number of R-279-000-315-597 and the Singapore National Research Foundation (NRF) support through the Competitive Research Program for the project entitled, "New Advanced FO membranes and membrane systems for wastewater treatment, water reuse and seawater desalination" with a grant number of R-279-000-336-281.

Notation

A_m = effective membrane surface area, m^2
C_0 = initial salt concentration of the feed, mol L^{-1}
C_f = solute concentration in the feed solution, mol L^{-1}
$C_{membrane}$ = concentration of NaCl in the dense membrane, mol L^{-1}
C_p = solute concentration in the permeate, mol L^{-1}
CP = concentration polarization
$C_{solution}$ = concentration of NaCl in the solution, mol L^{-1}
$C_{s,w}$ = final salt concentration in the water chamber, mol L^{-1}
$C_{s,s}$ = final salt concentration in the salt solution, mol L^{-1}
C_t = salt concentration in the feed after the operation time interval, mol L^{-1}
C_w = equilibrium water content, wt %
D_s = salt diffusion coefficient, m^2 s^{-1}
FO = forward osmosis
ICP = internal concentration polarization
J_s = salt flux, g m^{-2} h^{-1}
J_w = water flux, L m^{-2} h^{-1}
K_s = salt partition coefficient
Δm = weight change, kg
MD = membrane distillation
M_w = molecular weight of the draw solute, kg mol^{-1}
$MWCO$ = molecular weight cut off, Da
PRO = pressure retarded osmosis
PWP = pure water permeability, L m^{-2} h^{-1} bar^{-1}
R_E = effective solute rejection coefficient, %
Δt = the operation time interval, h
TFC = thin film composite
V_0 = initial volume of the feed, L
V_t = volume of the feed after the operation time interval, L
W_{air} = weight of the dense in air, kg
W_{liquid} = weight of the dense in the auxiliary liquid, kg
W_{dry} = weight of the dry membrane sample, kg
W_{wet} = weight of the wet membrane sample, kg
Δx = thickness of the membrane sample, m

Greek letters

ρ = density of the dense membrane, kg m^{-3}
ρ_0 = density of the auxiliary liquid, kg m^{-3}

Literature Cited

1. McCutcheon JR, McGinnis RL, Elimelech M. A novel ammonia-carbon dioxide forward osmosis desalination process. *Desalination.* 2005;174:1–11.
2. Choi YJ, Choi JS, Oh HJ, Lee S, Yang DR, Kim JH. Toward a combined system of forward osmosis and reverse osmosis for seawater desalination. *Desalination.* 2009;247:239–246.
3. Cornelissen ER, Harmsen D, de Korte KF, Ruiken CJ, Qin JJ, Oo H, Wessels LP. Membrane fouling and process performance of forward osmosis membranes on activated sludge. *J Membr Sci.* 2008;319:158–168.
4. Lay WCL, Zhang Q, Zhang J, McDougald D, Tang C, Wang R, Liu Y, Fane AG. Study of integration of forward osmosis and biological process: membrane performance under elevated salt environment. *Desalination.* 2011;283:123–130.
5. Kessler JO, Moody CD. Drinking water from sea water by forward osmosis. *Desalination.* 1976;18:297–306.
6. Lee KL, Baker RW, Lonsdale HK. Membranes for power generation by pressure-retarded osmosis. *J Membr Sci.* 1981;8:141–171.
7. Thorsen T, Holt T. Semi-permeable membrane for use in osmosis and method and plant for providing elevated pressure by osmosis to create power. U.S. Patent7,653,370 B2, 2007.
8. Yang Q, Wang KY, Chung TS. A novel dual-layer forward osmosis membrane for protein enrichment and concentration. *Sep Purif Technol.* 2009;69:269–274.
9. Phuntsho S, Shon HK, Hong S, Lee S, Vigneswaran S. A novel low energy fertilizer driven forward osmosis desalination for direct fertigation: evaluation the performance of fertilizer draw solutions. *J Membr Sci.* 2011;375:172–181.
10. Herron J. Asymmetric forward osmosis membranes. Hydration Technologies Inc. US7,445,712 B2, 2008.
11. Wang KY, Ong RC, Chung TS. Double-skinned forward osmosis membranes for reducing internal concentration polarization within the porous sublayer. *Ind Eng Chem Res.* 2010;49:4824–4831.
12. Qiu C, Setiawan L, Wang R, Tang CY, Fane AG. High performance flat sheet forward osmosis membrane with an NF-like selective layer on a woven fabric embedded substrate. *Desalination.* 2012;287:266–270.
13. Yang Q, Wang KY, Chung TS. Dual-layer hollow fibers with enhanced flux as novel forward osmosis membranes for water reclamation. *Environ Sci Technol.* 2009;43:2800–2805.
14. Yip NY, Tiraferri A, Phillip WA, Schiffman JD, Elimelech M. High performance thin-film composite forward osmosis membrane. *Environ Sci Technol.* 2010;44:3812–3818.
15. Qiu C, Qi S, Tang CY. Synthesis of high flux forward osmosis membranes by chemically crosslinked layer-by-layer polyelectrolytes. *J Membr Sci.* 2011;381:74–80.
16. Wang HL, Chung TS, Tong YW, Meier W, Chen Z, Hong M, Jeyaseelan K, Armugam A. Preparation and characterization of pore-suspending biomimetic membranes embedded with Aquaporin Z on carboxylated polyethylene glycol polymer cushion. *Soft Mater.* 2011;7:7274–7280.
17. Ge QC, Su JC, Chung TS, Amy G. Hydrophilic superparamagnetic nanoparticles: synthesis, characterization, and performance in forward osmosis processes. *Ind Eng Chem Res.* 2011;50:382–388.
18. Ling MM, Chung TS, Lu XM. Facile synthesis of thermosensitive magnetic nanoparticles as "smart" draw solutes in forward osmosis. *Chem Commun.* 2011;47:10788–10790.
19. Mi BX, Elimelech M. Organic fouling of forward osmosis membranes: fouling reversibility and cleaning without chemical reagents. *J Membr Sci.* 2010;348:337–345.
20. Li ZY, Yangali-Quintanilla V, Valladares R, Li Q, Zhan T, Amy G. Flux patterns and membrane foulding propensity during desalination of seawater by forward osmosis. *Water Res.* 2011;46:195–204.
21. Zhang S, Wang KY, Chung TS, Chen HM, Jean YC, Amy G. Well-constructed cellulose acetate membranes for forward osmosis: minimized internal concentration polarization with an ultra-thin selective layer. *J Membr Sci.* 2010;360:522–535.
22. Yu Y, Seo S, Kim IC, Lee S. Nanoporous polyethersulfone (PES) membrane with enhanced flux applied in forward osmosis process. *J Membr Sci.* 2011;375:63–68.
23. Hausman R, Digman B, Escobar IC, Coleman M, Chung TS. Functionalization of polybenzimidizole membranes to impart negative charge and hydrophilicity. *J Membr Sci.* 2010;363:195–203.
24. Wang KY, Chung TS, Qin JJ. Polybenzimidazole (PBI) nanofiltration hollow fiber membranes applied in forward osmosis process. *J Membr Sci.* 2007;300:6–12.
25. Su JC, Yang Q, Teo JF, Chung TS. Cellulose acetate nanofiltration hollow fiber membranes for forward osmosis processes. *J Membr Sci.* 2010;355:36–44.
26. Wang R, Shi L, Tang CY, Chou S, Qiu C, Fane AG. Characterization of novel forward osmosis hollow fiber membranes. *J Membr Sci.* 2010;355:158–167.
27. McCutcheon JR, Elimelech M. Influence of concentrative and dilutive internal concentration polarization on flux behavior in forward osmosis. *J Membr Sci.* 2006;284:237–247.
28. Verissimo S, Peinemann KV, Bordado J. New composite hollow fiber membrane for nanofiltration. *Desalination.* 2005;184:1–11.
29. Strathmann H. Membrane separation processes: current relevance and future opportunities. *AIChE J.* 2001;47:1077–1087.
30. Zhao S, Zou L, Mulcahy D. Brackish water desalination by a hybrid forward osmosis-nanofiltrtion system using divalent draw solute. *Desalination.* 2012;284:175–181.

31. Ling MM, Chung TS. Novel dual-stage FO system for sustainable protein enrichment using nanoparticles as intermediate draw solutes. *J Membr Sci*. 2011;372:201–209.
32. Wang KY, Teoh MM, Nugroho A, Chung TS. Integrated forward osmosis-membrane distillation (FO-MD) hybrid system for the concentration of protein solutions. *Chem Eng Sci*. 2011;66:2421–2430.
33. Kim Y, Oh D, Kim Y, Lee KH, Lee J. Development of a pilot-scale forward osmosis desalination process. AIChE Annual Meeting, Minneapolis, Oct. 17–21, 2011.
34. Yen SK, Haja N. FM, Su ML, Wang KY, Chung TS. Study of draw solutes using 2-methylimidazole based compounds in forward osmosis. *J Membr Sci*. 2010;364:242–252.
35. Su JC, Chung TS. Sublayer structure and reflection coefficient and their effects on concentration polarization and membrane performance in FO processes. *J Membr Sci*. 2011;376:214–224.
36. Soltanieh M, Gill WN. Review of reverse osmosis membranes and transport models. *Chem Eng Commun*. 1981;12:279–363.
37. Achilli A, Cath TY, Childress AE. Selection of inorganic-based draw solutions for forwards osmosis applications. *J Membr Sci*. 2010;364:233–241.
38. Stamatialis DF, Dias CR, de Pinho MN. Structure and permeation properties of cellulose esters asymmetric membranes. *Biomacromolecules*. 2000;1:564–570.
39. Chung TS, Teoh SK, Hu XD. Formation of ultrathin high-performance polyethersulfone hollow fiber membranes. *J Membr Sci*. 1997;133:161–175.
40. Sukitpaneenit P, Chung TS. Molecular elucidation of morphology and mechanical properties of PVDF hollow fiber membranes from aspects of phase inversion, crystallization and rheology. *J Membr Sci*. 2009;340:192–205.
41. Ong YK, Widjojo N, Chung TS. Fundamentals of semi-crystalline poly(vinylidene fluoride) membrane formation and its prospects for biofuel (ethanol and acetone) separation via pervaporation. *J Membr Sci*. 2011;378:149–162.
42. Bhongsuwan D, Bhongsuwan T. Preparation of cellulose acetate membranes for ultra-nanofiltrations. *Kasetsart J. (Nat. Sci.)* 2008;42:311–317.
43. Gekas V, Olund K. Mass transfer in the membrane concentration polarization layer under turbulent cross flow. II. Application to the characterization of ultrafiltration membranes. *J Membr Sci*. 1988;37:145–163.

Manuscript received Mar. 11, 2012, and revision received July 26, 2012.